JOURNAL OF THE MECHANICAL BEHAVIOR OF BIOMEDICAL MATERIALS 48 (2015) 183–191

Available online at www.sciencedirect.com

ScienceDirect

www.elsevier.com/locate/jmbbm

Research Paper

Biocompatibility and compressive properties of Ti-6Al-4V scaffolds having Mg element

Seyed Mohammad Kalantari[a,*], *Hossein Arabi*[b], *Shamsodin Mirdamadi*[b], *Seyed Ali Mirsalehi*[a]

[a]*Composite Laboratory, School of Materials Science and Engineering, Iran University of Science and Technology, Narmak, Tehran, 16846-13114, Iran*

[b]*Center of Excellence for High Strength Alloys Technology (CEHSAT), School of Materials Engineering, Iran University of Science and Technology, Narmak, Tehran, Iran*

ARTICLE INFO

Article history:
Received 24 December 2014
Received in revised form
13 March 2015
Accepted 10 April 2015
Available online 22 April 2015

Keywords:
Biocompatibility
Compressive properties
Ti-6Al-4 V
Scaffold
Mg

ABSTRACT

Porous scaffolds of Ti-6Al-4V were produced by mixing of this alloy with different amount of magnesium (Mg) powders. The mixtures were compacted in steel die by applying uniaxial pressure of 500 MPa before sintering the compacts in sealed quartz tubes at 900 °C for 2 h. Employing Archimedes' principle and Image Tool software, the total and open volume percentages of porosities within the scaffolds were found to be in the range of 47–64% and 41–47%, respectively. XRD results of titanium before and after sintering showed that no contamination, neither oxides nor nitrides formed during processes. Compressive properties of the scaffolds were studied using an Instron machine. The observed compressive strength and Young's module of the scaffolds were in the range of 72–132 MPa, and 37–47 GPa, respectively. Cell attachment and proliferation rate of MG-63 on porous samples were investigated. The results showed that proliferation rate increased with increasing Mg content. However no clear differences were observed between samples regarding cell attachment, so that bridges were observed in all cell gaps within the scaffolds.

1. Introduction

In contrast to the ceramic and polymeric biomaterials which possess poor mechanical properties, metallic biomaterials have been known as the most suitable materials for load-bearing applications (Arifvianto and Zhou, 2014). Titanium (Ti) and its alloys are nowadays the most attractive metallic biomaterials due to their good mechanical properties, unique biocompatibility, and high corrosion resistance among all other metals (Ryan et al., 2009; Oshida, 2010; Ayda et al., 2005; Dezfuli et al., 2012; Li et al., 2005; Kotan and Bor, 2009). However, the major limitation concerning metallic implants in orthopedic surgery is the mismatch of elastic module between the bone (0.1–30 GPa) and metallic implants (110 GPa for Ti) following the stress shielding and bone resorption over time (Ryan et al., 2006; Chen et al., 2009; Kim et al., 2013; Niinomi, 1998; Zhang et al., 2013; de Vasconcellos et al., 2012). One solution to solve this problem in medical applications has been the development of

*Corresponding author. Tel.: +98 217 724 0540.
E-mail address: kalantary.mohammad@gmail.com (S.M. Kalantari).

http://dx.doi.org/10.1016/j.jmbbm.2015.04.015
1751-6161/

materials that exhibit substantial surface or high total bulk porosity (Ryan et al., 2006).

The fabrication techniques of porous metals are classified into four groups of production: liquid, solid, gas, and aqueous solutions. Due to high activity of titanium with atmosphere gases at molten state, most of the production methods are not adequate (de Vasconcellos et al., 2012; Mansourighasri et al., 2012). Among these methods, the simplest fabrication technique for producing porous metal is powder metallurgy (PM) route which is widely used due to its considerable advantages such as low cost, better control and the capability of near-net-shape production (Mansourighasri et al., 2012).

Pore sizes and shapes obtained in PM are a function of powder size and shape as well as the shape and size of space holder (Jha et al., 2013). Conventional space holders are carbamide, sodium chloride, ammonium hydrogen carbonate, and magnesium (Arifvianto and Zhou, 2014; Mansourighasri et al., 2012; Jha et al., 2013; Smorygo et al., 2012). Among these space holders Mg could be a good candidate in titanium scaffolds production, since its solubility in titanium is expected to be negligible. Furthermore it enhances osteoconductivity of scaffolds if it remains and does not constitute a drawback for biomedical applications (Aydoğmuş and Bor, 2009). Therefore, employing magnesium as a space holder and its incomplete removal from the scaffold can result to fabrication of porous structure and promotes its biocompatibility, simultaneously.

In present study, porous Ti-6Al-4V/Mg foam was fabricated by powder metallurgical process for bone substitute applications. Mechanical and biocompatibility properties of these fabricated metallic scaffolds are described in this article.

2. Materials and methods

2.1. Materials preparation

Residual spring-like chips from machining process of Ti-6Al-4V bars were used as starting material. Quantometer analysis was used to determine the chemical composition of the as-received chips from raw Ti-6Al-4V bar (Table 1). Similar chemical composition to that standard specification for Ti-6Al-4V powders used for coating surgical and medical implants (ASTM F1580-01, 2001) was obtained.

Since the spring-like chips filled up the most of vial volume, i.e., preventing balls to move effectively in a milling process, they were manually crushed in a mortar prior to milling to obtain small pieces with a length less than 1 cm.

In order to crush chips to much smaller pieces planetary ball milling machine (Retsch PM400 type) under protective atmosphere of argon (Ar) (99.998% pure) was used. The powder was ground in a tungsten carbide closed vial. The powder to ball mass ratio was about 1:10 with a milling speed of 250 rpm at room temperature. The milling operation was performed for 6 h in such a way that the rotary machine was on for 20 min and 10 min off for cooling. Ethanol was added to the vials to act as a coolant and prevent excessive heat generation during ball milling. The crystal structure of the as milled powder was characterized by means of X-ray diffraction (Philips X'PERT MPD) using filtered Cu Kα radiation (k=0.1542 nm).

2.2. Fabrication of scaffold

Ti-6Al-4V and magnesium (Merck > 99% pure) powders were sieved separately to obtain a powder range of 37–90 μm for the alloy and 90–180 μm for Mg powders. Then various amounts of Mg powders (i.e., 30, 45, and 60 vol% Mg) were mixed with the alloy powder in an agate mortar using 5 wt% polyvinyl alcohol (PVA) solution (5 wt% PVA+95 wt%water) as the binder prior to compaction. PVA solution was required for coating of coarse Mg particles with fine Ti-6Al-4V powders uniformly. Mixing time was determined as 30 min to assure a homogeneous distribution of powders. Then the mixtures were uniaxially pressed at a pressure of 500 MPa in a steel die using a hydraulic press. The heat treatment process consisted of two steps, i.e., at 450 °C for 2 h to allow debinding of PVA and then 900 °C for 2 h for sintering. Production steps involved in the space holder technique applied are summarized in Fig. 1. Argon flow rate was kept at a minimum adequate to provide a positive internal pressure inside the furnace to avoid possible leakage of air into the furnace. Samples were placed in a quartz tube in order to reduce evaporation of magnesium. The main phases in the scaffold were identified by X-Ray Diffraction (XRD Philips X'PERT MPD) analysis using a Cu-Kα radiation source.

2.3. Pore characterization

The amounts of porosity in Ti-6Al-4V/Mg scaffolds were determined via Archimedes' principle according to ASTM B328 standard. Total porosity was evaluated by image analyzer attached to an optical microscope and suitable analyzing software (Image Tool). For the image analysis, a sequence of conventional metallographic steps was carried out on the sectioned parts.

2.4. Mechanical testing

Compression tests were carried out on cylindrical scaffolds with diameter and height of 10 mm at ambient temperature (25 °C) at a constant cross-speed of 0.5 mm/min^{-1} employing an Instron-1185 universal test machine. Three specimens were tested at each porosity level to compensate the possible

Table 1 – Mean chemical composition of Ti-6Al-4V bar (wt%).

Element	Ti	Al	V	Cu	Mo	Sn	Si	Fe	Zr	Mn	C
Wt%	88.04	6.33	4.99	0.01	0.02	0.00	0.00	0.48	0.00	0.01	0.77
ASTM F1580-01	Balance	5.5–6.75	3.5–4.5	0.1	–	0.1	–	0.3	–	–	0.8

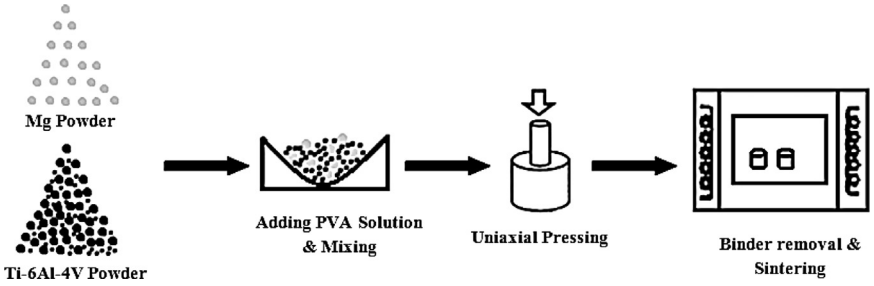

Fig. 1 – Schematic of processing steps for fabricating scaffolds.

scattering of the results. The average compressive strength for each specimen was determined. The elastic moduli of the specimens were also calculated from the stress strain curves fitted to the linear elastic regions.

2.5. *Cell culture*

Prior to cell culture, the porous samples were cleaned and sterilized in order to create a clean surface for cell proliferation. Each sample was cleaned ultrasonically in acetone, 100% ethanol and deionized water for 15 min. They were then dried with a hair-dryer and subsequently autoclaved at 121 °C under a pressure of 1.5 Kg/cm^2 for 1 h before placing them in multi-well culture plates.

MG-63 human osteosarcoma cell lines (NCBI C-555, National Cell Bank of Iran, Pasteur Institute of Iran) were cultured at a density of 1×10^4 cells on the surface of each sample. MG-63 cells were cultured in Dulbecco's Modified Eagle's Medium (DMEM; GIBCO, Scotland) supplemented with 10% fetal bovine serum (FBS, Gibco), 100 U/mL penicillin, and 100 μg/mL streptomycin (Sigma, U.S.A.). MG-63 cells were harvested with 0.25% trypsin-EDTA solution (Sigma) in phosphate buffered saline (PBS, pH 7.4). According to the ISO 10993-5, MG-63 cells were incubated at 37 °C in humidified air with 5% CO_2 for a period of 7 days. The cultured medium was changed every two days without making disturbance in culture conditions.

Cell culture tests were carried out on cylindrical specimens with diameter of 10 mm and height of 5 mm. Three samples were used for each group and in-vitro assays repeated three times for each scaffold.

2.5.1. *Cell morphology*

Morphology of cells attached to samples was studied using SEM. MG-63 cells at a density of 5×10^3 cells/well in 24-well plates were placed on each scaffolds. The plates were incubated at 37 °C in humidified air containing 5% CO_2. 2.5% glutaraldehyde buffered in 0.2 M phosphate-buffered saline (PBS) was used for fixing cells after 6 h of incubation period. Graded alcohols (50, 70, 90, 95, and 100%) were used for dehydrating specimens. Dehydration was carried out by air drying for 24 h. The specimens were observed using SEM after sputtering a gold layer.

2.5.2. *Proliferation of MG-63 cells*

Dimethylthiazol diphenyl tetrazolium bromide (MTT) assay was used for evaluation proliferation rate of osteoblast cells. Briefly, MG-63 cultured cells were suspended in culture medium at a density of 1×10^3 cells/50 μL and were added to each of the wells in the 96-microtiter plates (NUNC, Denmark).The plates were incubated at 37 °C in a humidified atmosphere of 5% CO_2 in air for 24 h. One tissue culture polystyrene (TPS) well used as a control. The plates containing scaffolds and the cells were incubated at 37 °C with 5% CO_2 for 7 days. Every two days, cultured medium was changed. At predetermined intervals, scaffolds were taken out of wells. 100 μl of MTT (5 mg/mL in medium) was added to each of the wells and incubated for another 4 h at 37 °C in a humidified atmosphere of 5% of CO_2 in air. At this stage the MTT was removed and the formazan crystals were dissolved by adding 100 μL of isopropanol (Sigma) in each well. The plates were placed in the incubator for 10 min and then in a cold room for 15 min prior to absorbance measurements. Multiwell microplate reader (ICN, Switzerland) was used for reading optical density (OD) of each well at 545 nm wavelengths. The experiment was repeated three times.

2.5.3. *Statistical analysis*

Each of the experimental points reported in this work is an average value taken out of three measurements. The standard deviations are used as error bars in the figures and tables.

Statistical analysis was carried out using Sigmaplot v.6 soft-ware (SPSS Inc). Data are reported as mean ± standard deviation (SD) at a significance level of $p<0.05$. Differences were considered statistically significant when the p-Value was <0.05.

3. Results and discussion

3.1. *X-ray diffraction*

Fig. 2a, illustrates the result of X-ray diffraction of ball milled alloy powder. The XRD spectrum reveals that the ball milled powder is mainly Ti-6Al-4V. Although titanium is very reactive element and prone to form various oxides and nitrides such as TiO_2 and TiN, neither oxides nor nitrides were detected after ball milling such that all diffracted peaks are related to Ti-6Al-4V.In comparison with using steel container and steel ball which induce Fe contamination (Mahboubi Soufiani et al., 2010), in this process no intermetallic compound formed during ball milling when tungsten carbide vial was used. This phenomenon can be attributed to higher friction coefficient of tungsten carbide compared to steel ball.

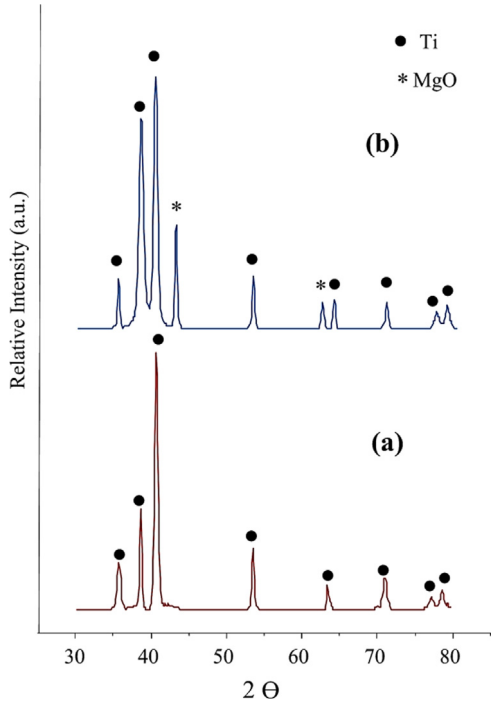

Fig. 2 – The results of X-ray diffraction analysis of the (a) prepared Ti-6Al-4V powders and (b) scaffold with 45 vol% of Mg after sintering.

Table 2 – Pore characterizations extracted from software Image Tool and use of Archimedes' principle.

Sample	Total porosity (%)	Open porosity (%)
Ti6Al4V/30Mg	47±6	41±8
Ti6Al4V/45Mg	54±5	43±6
Ti6Al4V/60Mg	64±10	47±13

3.2. *Characterization of porosity and pores*

The results of the image analysis together with Archimedes' principle for specimens are summarized in Table 2. The results of image analysis show that the amounts of total and open porosities tend to increase from 47% and 41% to 64% and 47%, respectively, with increasing the magnesium content. The open pores are identified as the percentage of the interconnected pore spaces within the total porosities. According to Fig. 3, two types of pores were observed after sintering. One was the small pore having several micrometers mean diameters were inherited from the spaces among Ti-6Al-4V particles after compaction, while the large pores were generated after the partial evaporation of magnesium. Porosities within the scaffolds that manufactured by partial evaporation of magnesium were mostly open type pores. The sizes and shapes of pores were dictated by the sizes and shapes of original powders used. Typical pore morphologies of the scaffolds surfaces with different amounts of magnesium are illustrated in Fig. 4. As it can be seen in Fig. 4, pores shapes are irregular and have different sizes due to the irregular shapes and inconsistent sizes of Mg particles. It should be noted that compacts having

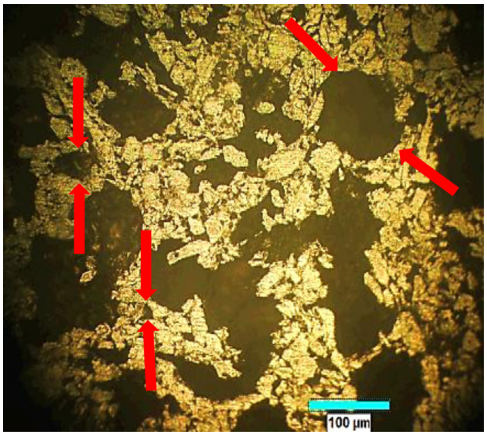

Fig. 3 – Micro and macro pores after the partial evaporation of Mg from scaffold.

greater than 20 vol% porosity are considered as promising samples for biomedical (Oh et al., 2003).

X-ray diffractograms of fabricated scaffold which had 45 vol% of Mg before sintering, displayed in Fig. 2b. Diffraction patterns of the sample, contain only peaks of titanium and magnesium oxide. The presence of MgO is due to the high-chemical activity of Mg which provides a reducing atmosphere that prevents oxidation of Ti-6Al-4V during sintering. XRD patterns reveal that there was no reaction between the two original components, i.e., magnesium and titanium, during the sintering process. In fact Mg solubility in titanium is expected to be negligible, so that biocompatibility properties would not be affected. In addition, Mg can be dissolves in the body and forms compounds that are non-toxic in small quantities. These criteria have made magnesium the best choice as space holder and also osteoconductive element in titanium alloy scaffold production.

After sintering, the surface of the sample with 45 vol% of Mg before sintering was analyzed by Energy-dispersive X-ray Spectrometry (EDS) and the result is presented in Fig. 5. These spectrographs show the presence of magnesium and titanium in scaffold. Also, Si detected in EDS analysis due to mechanical grinding of samples with SiC paper for removing surface oxides. According to Fig. 5, the amount of Si is low and it does not adversely affect mechanical and biocompatibility properties. Typical distribution of titanium and magnesium on the surface of the sample is shown in Fig. 5. The amount of magnesium within the porous areas are more than those observed on the smooth surfaces which is an indication of the presence of more Mg in these area which caused the formation of large number of porosity due to its partial evaporation during sintering resulting to an increase in biocompatibility properties insides pores.

3.3. *Compressive behavior*

Fig. 6 presents typical compressive stress–strain curves of the scaffolds having different amounts of porosities. Compressive properties of the scaffolds are summarized in Table 3. Obviously, the compressive strength and Young's modulus of the samples are inversely correlated with the porosity level. The scaffolds with approximately 47, 54, and 64% porosity exhibited, the compressive strength of 132, 96, and 72 MPa and

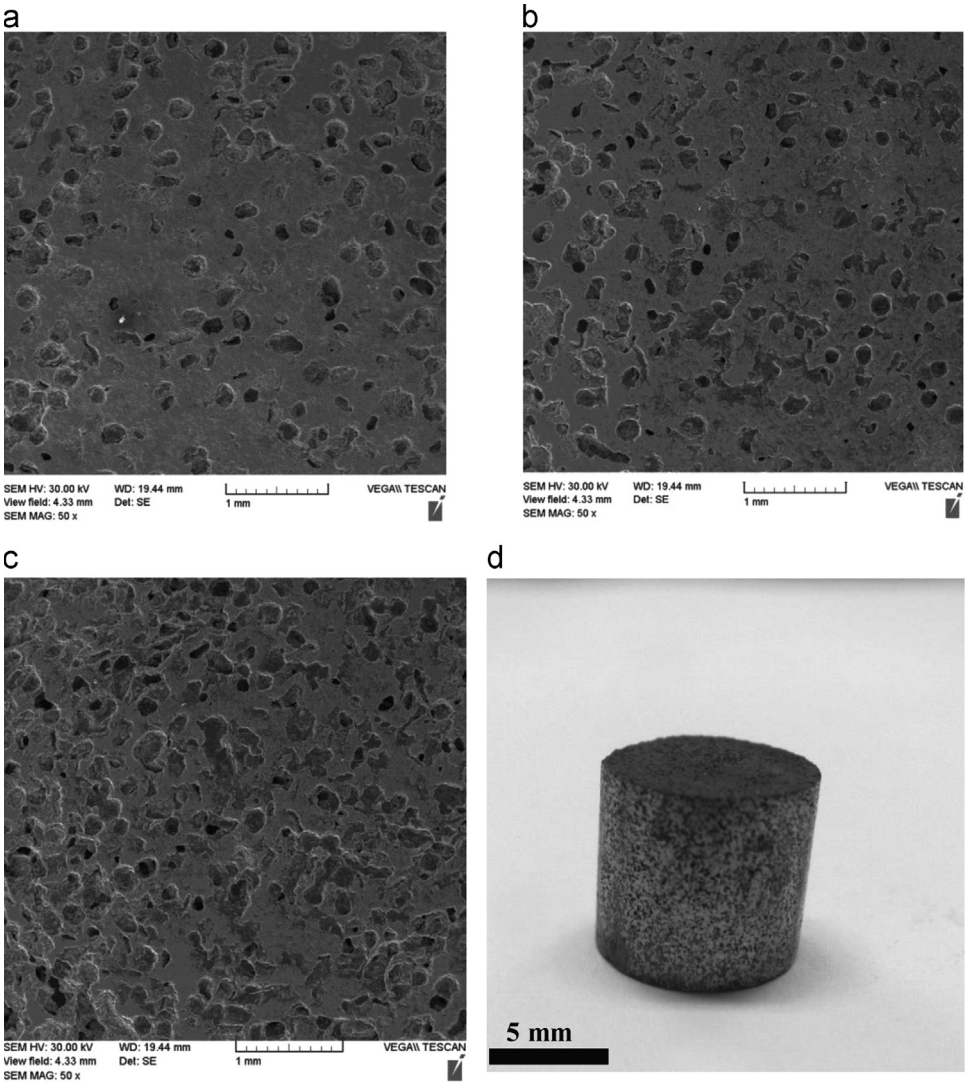

Fig. 4 – Pore morphology in Ti-6Al-4V scaffold's surface having: (a) 30, (b) 45, and (c) 60 vol% Mg. A typical macro-photo of the Ti-6Al-4V/Mg scaffold can be seen in (d).

Young's modulus of 47, 41, and 37 GPa, respectively. The compressive stress–strain curves exhibited reasonably large total amounts of strains. However the linear strains in all of the samples are low and failed in pseudo-brittle mode which is the major problem of these fabricated Ti-6Al-4V scaffolds. The embrittlement of the porous samples might be attributed to the sintering temperature. According to Gagg et al., (2013) when the temperature of sintering is low and very close to the α to β phase transition point (i.e., 882 °C) formation of brittle ω phase has been observed. This phase prevents enough consolidation between adjacent particles and promote brittle behavior (İpek Nakaş et al., 2011). Furthermore due to weak interface bonding between Mg and Ti-6Al-4V particles and no information of intermetallics, they have no effect on the mechanical properties of the scaffolds (Umeda et al., 2010).

A typical compression stress–strain curve of the specimens can be divided into four distinct deformation regions marked as I, II, III, and IV on Fig. 6b. In region I, the compact is elastically compressed up to about the proportional limit at the beginning of deformation. According to observations of Tscdemirci et al., (2008) after the proportion limit and before maximum compressive strength, shear bands starts to propagate along the diagonal axes of the scaffolds at 45° to the compression direction. In this region inelastic deformation under normal and shear forces begins to become non-uniform. In region III, reduction in the load carrying capacity takes place as a consequence of deformation localization in the shear bands. In region IV, fluctuation of stress values occurs around a constant stress as a result of shearing the two cone apices on top of each other (Fig. 7) according to Tscdemirci et al., (2008). Particle separation along the diagonal axes beginning from the corners of the cylindrical scaffold at strains of about 12% leads to complete failure.

The elastic modulus range of cancellous and cortical human bones is 0.01–1.57 GPa and 7–30 GPa, respectively (Mirsalehi et al., 2015; Norman et al., 2008). In the present study, the constant stress in region IV has not been observed in scaffold with 30 vol% Mg, while this region appeared in the other two samples (Fig. 6). According to Table 3, Young's module of Ti-6Al-4V/30 vol% Mg sample (47 GPa) is more than

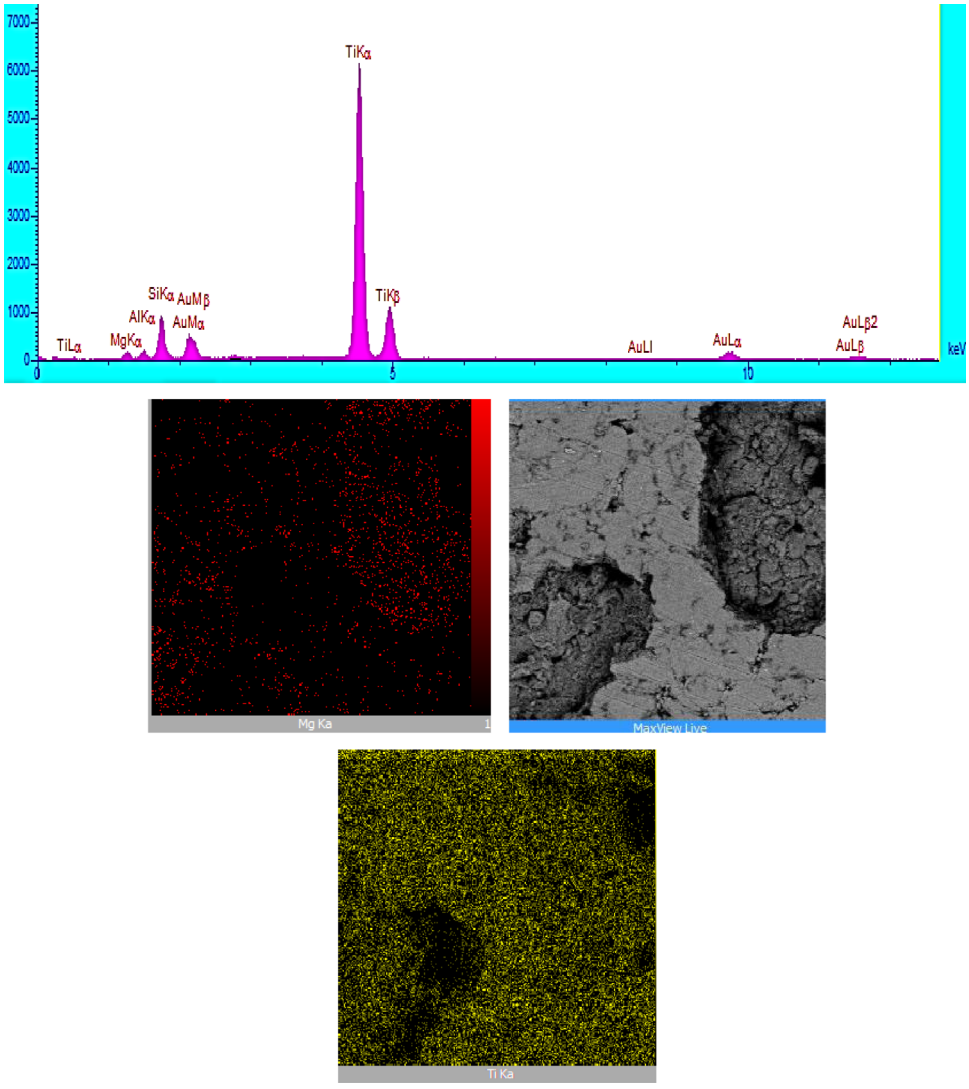

Element	Weight Percent %	Atomic Percent %
Mg	3.12	6.11
Al	2.55	4.51
Si	9.22	15.64
Ti	70.60	70.23
Au	14.50	3.51
Total	100	100

Fig. 5 – EDS analysis of the scaffold with 45 vol% of Mg and distribution of Ti and Mg on the surface of scaffold.

cancellous bone and close to cortical human bone. Therefore, this sample is not suitable for cancellous human bone substitution due to the high mismatch of elastic modulus between it and spongy bone, which will leads to the stress shielding effect. Hence, scaffold with 30 vol% Mg and 47% porosity appears to be appropriate for cortical bone replacement applications not only for its lower strain but for its higher elastic modulus. Scaffolds with greater porosities, on the other hand, seems not to be suitable for load bearing biomedical applications due to their insufficient strengths and higher elongation. Therefore, all the samples exhibited considerably higher strain than 7% are seem to be suitable for cancellous bone according to Aydoğmuş and Bor, (2009).

3.4. *In vitro assays*

The cells attachment of the MG-63 cell on the surfaces of samples was observed by SEM. SEM images of the extent of cell ingrowth into the porous Ti-6Al-4V structures (Fig. 8) showed that different amounts of Mg are associated with different pores, so the more the volume fraction of the pores with higher Mg content, the more will be the extent of the cell ingrowth, helping the formation of bridge across the pores.

It is thought that the membrane-associated adhesion receptors which belong to the integrin superfamily play a crucial role in mediating cellular interactions between osteoblasts and the biomaterial surface (Zreiqat et al., 2002).

Functional integrins are transmembrane heterodimers consisting of non-covalently associated α and β subunits (Anselme, 2000). Some divalent cations such as Mg^{2+}, Ca^{2+}, Mn^{2+} could bind motifs which are a part of the extracellular domain of the-subunit and integrin affinity to their respective ligands will be modified due to extracellular changes in these ions (Zreiqat et al., 2002). Thus in the presence of Mg within the pores, cells were frequently observed to spread on the surfaces of the particles and bridge the pores as it can be seen in Fig. 8.

The cellular behavior is affected by porous materials due to various factors such as pore size. The effect of pore size on cell ingrowth and bridging can be described by hypothetical mechanism presented by Chen et al., (2010). They stated that cells prefer to spread on both sides of the gaps between the particles, when a gap is too wide for one cell to bridge. Such attached cells provide closer surfaces for new born cells to attach on them and bridging the gap will be much easier. This process might take place again and again to cover a wide gap by new born cells which bridged by touching the ligands of existing cells. In contrast to wide gap which takes a lot of time for cell bridging and ingrowth, for a narrow gap, the initial attached cells are able to bridge the gap resulting in faster subsequent cell spreading and also leads to faster coverage of the pores by new cells.

Thus it is obvious that pore size is one of the most important factor which affects cell attachment. In Xue et al., (2007) it was declared that the human osteoblasts could only bridge pores smaller than 200 μm. Recent studies (Tian et al., 2012) have shown that pores with smaller size could be beneficial to osteoblastic attachment, proliferation and differentiation. It has been reported (Tian et al., 2012) that MG63 cells with a diameter of 30 μm have the ability to stretch well in the pores having a size of about 30 μm. In fact it is easier for cells to migrate and settle into the pores with the size equal to themselves (Tian et al., 2012). It can be observed in Fig. 8, where the diameter of pores are less than 30 μm, MG-63 cells exerted good stretching ability and bridged the pores.

The results of MTT assay after 7 day incubation are shown in Fig. 9. Viability percentage of each scaffold was measured three times and the mean values were used for comparison. The samples did not show any toxic effects. The difference between the values obtained from scaffolds could be due to the amount of porosities in the scaffolds. Bhattarai et al., (2008) have shown that higher amount of porosity ends up with greater proliferation rate. Fig. 9 exhibits that the cell

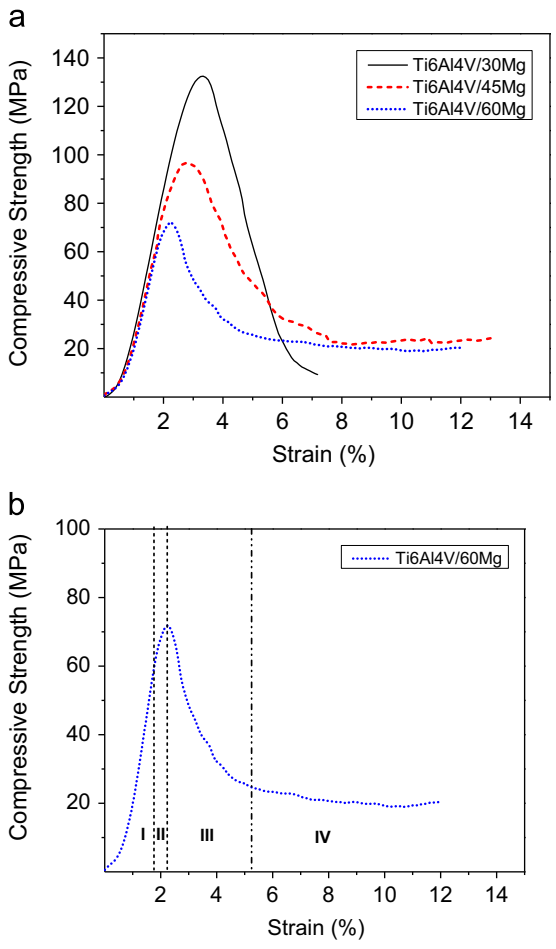

Fig. 6 – (a) Typical compressive stress versus strain of the porous Ti-6Al-4V scaffolds produced with various initial Mg contents (30, 45, and 60 vol%), (b) the compressive stress–strain curve of scaffold having 60 vol% Mg with four different deformation regions.

Fig. 7 – The typical ruptured section of compressed sample with the inverse V-shape.

Table 3 – Mechanical properties of porous Ti-6Al-4V samples tested in compression. The values given together with the standard deviations are average of three tests.

Sample	Young's module (GPa)	Compression strength (MPa)
Ti6Al4V/30 vol% Mg	47±4	132±10
Ti6Al4V/45 vol% Mg	41±3	97±7
Ti6Al4V/60 vol% Mg	37±2	72±5

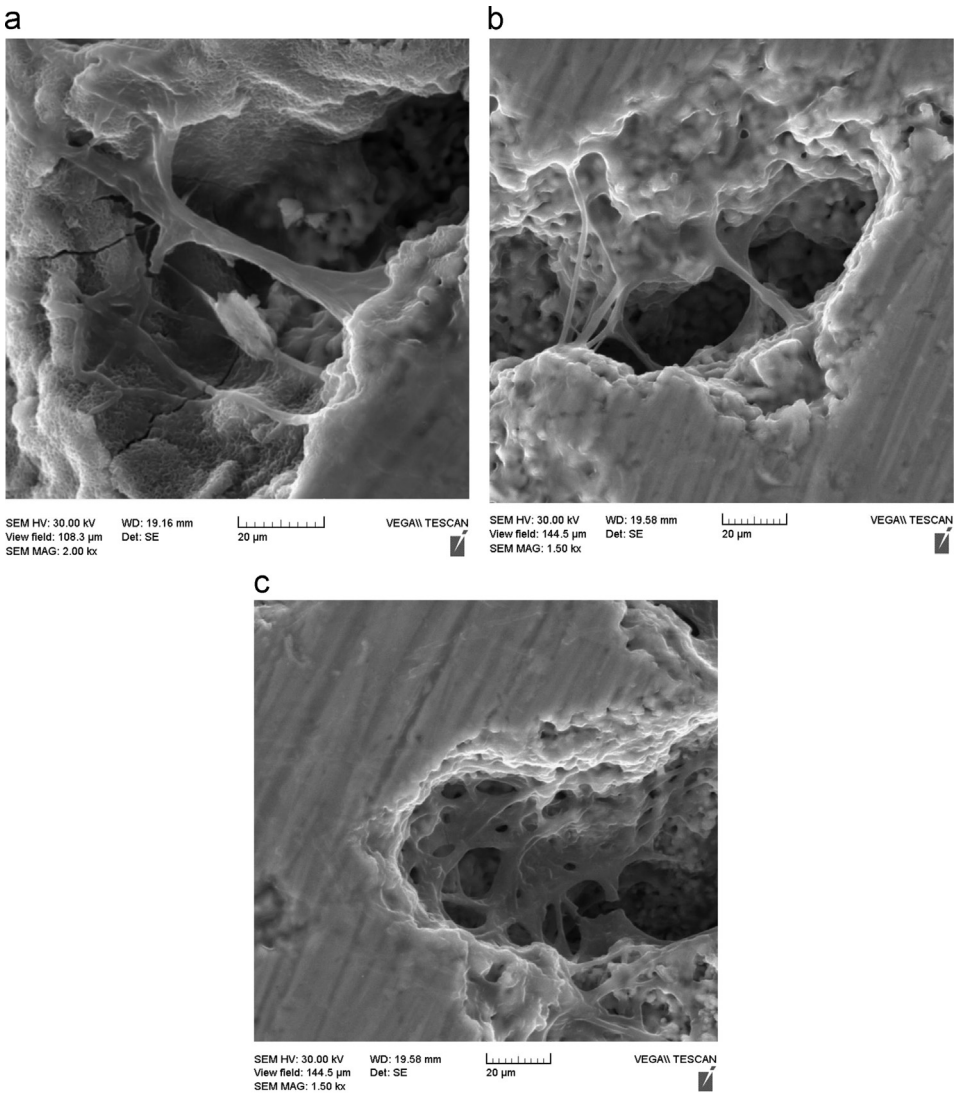

Fig. 8 – SEM micrograph of MG-63 cells attached to the scaffold's surface having: (a) 30, (b) 45, and (c) 60 vol % Mg after 6 h.

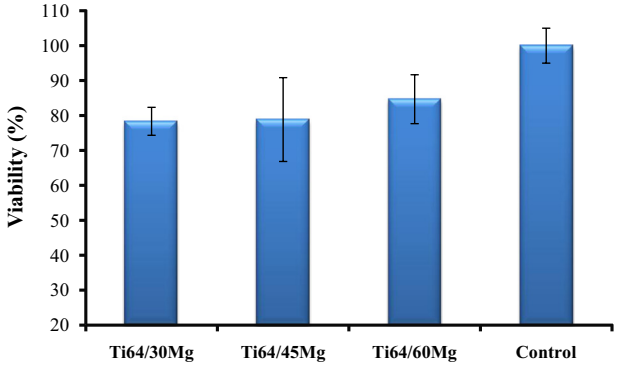

Fig. 9 – MG-63 osteoblast cell proliferation on porous scaffolds after 7 days.

proliferation was higher on 60 vol% Mg than on 45 and 30 vol % Mg in porous Ti-6Al-4V, in agreement with the observations of Li et al., (2007). In sample with 64% porosity, cells could migrate faster inside the pores of scaffold since pore space increased with porosity and facilitated transport of nutrients and oxygen. In fact higher amount of porosity did not affect cell attachment, but it can lead to an increase in cell proliferation. This observation has also been reported by Takahashi and Tabata, (2004).

4. Conclusions

Ti-6Al-4V scaffolds having different amounts of magnesium were successfully fabricated by a powder metallurgy technique. Partial evaporation of magnesium during sintering caused the formation of evenly distributed pores within the scaffold. The following conclusions are drawn:

1) The scaffolds have total and open porosities in the range of 47–64 vol% and 41–47 vol%, respectively. The pores formed via partial evaporation of magnesium during sintering.
2) The compressive strength and elastic modulus of the porous samples decrease significantly with increasing the amount of Mg. Mechanical properties at the porosity of around 47 vol % are found to be with those of human cortical bone.

3) MG63 cells, with the diameter of 30 μm, showed exerted good stretching ability in the pores with the size of 30 μm, inferring that the cells could migrate and settle into the pores with the size equal to them.
4) The porous structures with more amount of Mg have higher proliferation rates. This could be attributed to an increase in porosity with increasing Mg content.

REFERENCES

ASTM F1580-01, 2001. Standard Specification for Titanium and Titanium-6 Aluminum-4 Vanadium Alloy Powders for Coatings of Surgical Implants.

Anselme, K., 2000. Osteoblast adhesion on biomaterials . Biomaterials 21, 667–681.

Arifvianto, B., Zhou, J., 2014. Fabrication of metallic biomedical scaffolds with the space holder method: a review. Materials 7, 3588–3622.

Ayda, N., Alam, M., Ravindranath, M., 2005. Corrosion in titanium dental implants: literature review. J. Indian Prosthodonic Soc. 5, 126–131.

Aydoğmuş, T., Bor, Ş., 2009. Processing of porous TiNi alloys using magnesium as space holder. J. Alloy. Compd. 478, 705–710.

Bhattarai, S.R., Khalil, K.A.R., Dewidar, M., Hwang, P.H., Yi, H.K., Kim, H.Y., 2008. Novel production method and in-vitro cell compatibility of porous Ti-6Al-4V alloy disk for hard tissue engineering. J. Biomed. Mater. Res. A 86, 289–299.

Chen, J., Paetzell, E., Zhou, J., Lyons, L., Soboyejo, W., 2010. Osteoblast-like cell ingrowth, adhesion and proliferation on porous Ti-6Al-4V with particulate and fiber scaffolds. Mater. Sci. Eng. C 30, 647–656.

Chen, Y., Feng, B., Zhu, Y., Weng, J., Wang, J., Lu, X., 2009. Fabrication of porous titanium implants with biomechanical compatibility. Mater. Lett. 63, 2659–2661.

de Vasconcellos, L.M.R., Cairo, C.A.A., de Vasconcellos, L.G.O., de Alencastro Graça, M.L., do Prado, R.F., Carvalho, Y.R., 2012. Porous Titanium by Powder Metallurgy for Biomedical Application: Characterization, Cell Citotoxity and in vivo Tests of Osseointegration, INTECH Open Access Publisher, http://dx.doi.org/10.5772/47816.

Dezfuli, S.N., Sadrnezhaad, S., Shokrgozar, M., Bonakdar, S., 2012. Fabrication of biocompatible titanium scaffolds using space holder technique. J. Mater. Sci. Mater. Med. 23, 2483–2488.

Gagg, G., Ghassemieh, E., Wiria, F.E., 2013. Effects of sintering temperature on morphology and mechanical characteristics of 3D printed porous titanium used as dental implant. Mater. Sci. Eng. C 33, 3858–3864.

İpek Nakaş, G., Dericioglu, A.F., Bor, Ş., 2011. Fatigue behavior of TiNi foams processed by the magnesium space holder technique. J. Mech. Behav. Biomed. Mater. 4, 2017–2023.

Jha, N., Mondal, D., Dutta Majumdar, J., Badkul, A., Jha, A., Khare, A., 2013. Highly porous open cell Ti-foam using NaCl as temporary space holder through powder metallurgy route. Mater. Des. 47, 810–819.

Kim, S.W., Jung, H.-D., Kang, M.-H., Kim, H.-E., Koh, Y.-H., Estrin, Y., 2013. Fabrication of porous titanium scaffold with controlled porous structure and net-shape using magnesium as spacer. Mater. Sci. Eng. C 33, 2808–2815.

Kotan, G., Bor, A.Ş., 2009. Production and characterization of high porosity Ti-6Al-4V foam by space holder technique in powder metallurgy. Turk. J. Eng. Environ. Sci. 31, 149–156.

Li, J., De Wijn, J., Van Blitterswijk, C., De Groot, K., 2005. Porous Ti6Al4V scaffolds directly fabricated by 3D fibre deposition technique: effect of nozzle diameter. J. Mater. Sci. Mater. Med. 16, 1159–1163.

Li, J.P., Habibovic, P., van den Doel, M., Wilson, C.E., de Wijn, J.R., van Blitterswijk, C.A., de Groot, K., 2007. Bone ingrowth in porous titanium implants produced by 3D fiber deposition. Biomaterials 28, 2810–2820.

Mahboubi Soufiani, A., Enayati, M., Karimzadeh, F., 2010. Fabrication and characterization of nanostructured Ti6Al4V powder from machining scraps. Adv. Powder Technol. 21, 336–340.

Mansourighasri, A., Muhamad, N., Sulong, A., 2012. Processing titanium foams using tapioca starch as a space holder. J. Mater. Process. Technol. 212, 83–89.

Mirsalehi, S.A., Khavandi, A., Mirdamadi, S., Naimi-Jamal, M.R., Kalantari, S.M., 2015. Nanomechanical and tribological behavior of hydroxyapatite reinforced ultrahigh molecular weight polyethylene nanocomposites for biomedical applications. J. Appl. Polym. Sci. 132, 42052.

Niinomi, M., 1998. Mechanical properties of biomedical titanium alloys. Mater. Sci. Eng. A 243, 231–236.

Norman, J., Shapter, J.G., Short, K., Smith, L.J., Fazzalari, N.L., 2008. Micromechanical properties of human trabecular bone: a hierarchical investigation using nanoindentation. J. Biomed. Mater. Res. A 87, 196–202.

Oh, I.-H., Nomura, N., Masahashi, N., Hanada, S., 2003. Mechanical properties of porous titanium compacts prepared by powder sintering. Scr. Mater. 49, 1197–1202.

Oshida, Y., 2010. Bioscience and Bioengineering of Titanium Materials. Elsevier, Oxford.

Ryan, G., Pandit, A., Apatsidis, D.P., 2006. Fabrication methods of porous metals for use in orthopaedic applications. Biomaterials 27, 2651–2670.

Ryan, G., McGarry, P., Pandit, A., Apatsidis, D., 2009. Analysis of the mechanical behavior of a titanium scaffold with a repeating unit-cell substructure. J. Biomed. Mater. Res. Part B Appl. Biomater. 90, 894–906.

Smorygo, O., Marukovich, A., Mikutski, V., Gokhale, A., Reddy, G.J., Kumar, J.V., 2012. High-porosity titanium foams by powder coated space holder compaction method. Mater. Lett. 83, 17–19.

Takahashi, Y., Tabata, Y., 2004. Effect of the fiber diameter and porosity of non-woven PET fabrics on the osteogenic differentiation of mesenchymal stem cells. J. Biomater. Sci. Polym. Ed. 15, 41–57.

Tian, Y., Ding, S., Peng, H., Lu, S., Wang, G., Xia, L., Wang, P., 2012. Osteoblast growth behavior on porous-structure titanium surface. Appl. Surf. Sci. 261, 25–30.

Tscdemirci, A., Hızal, A., Altındiş, M., Hall, I., Güden, M., 2008. The effect of strain rate on the compressive deformation behavior of a sintered Ti6Al4V powder compact. Mater. Sci. Eng. A 474, 335–341.

Umeda, J., Kawakami, M., Kondoh, K., Ayman, E.-S., Imai, H., 2010. Microstructural and mechanical properties of titanium particulate reinforced magnesium composite materials. Mater. Chem. Phys. 123, 649–657.

Xue, W., Krishna, B.V., Bandyopadhyay, A., Bose, S., 2007. Processing and biocompatibility evaluation of laser processed porous titanium. Acta Biomater. 3, 1007–1018.

Zhang, X., Zheng, G., Wang, J., Zhang, Y., Zhang, G., Li, Z., Wang, Y., 2013. Porous Ti6Al4V scaffold directly fabricated by sintering: preparation and in vivo experiment. J. Nanomater. 2013, 18.

Zreiqat, H., Howlett, C., Zannettino, A., Evans, P., Schulze-Tanzil, G., Knabe, C., Shakibaei, M., 2002. Mechanisms of magnesium-stimulated adhesion of osteoblastic cells to commonly used orthopaedic implants. J. Biomed. Mater. Res. 62, 175–184.